PRAMANA
— journal of
physics

Vol. 72, No. 5
May 2009
pp. 833–844

Electric field distribution and simulation of avalanche formation due to the passage of heavy ions in a parallel grid avalanche counter

D KANJILAL and S SAHA*
Nuclear & Atomic Physics Division, Saha Institute of Nuclear Physics, Kolkata 700 064, India
*Corresponding author. E-mail: satyajit.saha@saha.ac.in; satyajit.saha12@gmail.com

MS received 6 August 2008; revised 20 February 2009; accepted 26 February 2009

Abstract. Electric field distributions and their role in the formation of avalanche due to the passage of heavy ions in parallel grid avalanche type wire chamber detectors are evaluated using a Monte Carlo simulation. The relative merits and demerits of parallel and crossed wire grid configurations are studied. It is found that the crossed grid geometry has marginally higher gain at larger electric fields close to the avalanche region. The spatial uniformity of response in the two wire grid configurations is also compared.

Keywords. Avalanche propagation; gas gain; parallel grid avalanche counter.

PACS Nos 29.40.Cs, 51.50.+v, 52.80.Dy

1. Introduction

Multiwire detectors have evolved into several configurations depending on the physics goal of the experiments. In the pioneering work of George Charpak *et al* [1], the detector was developed for high energy physics experiments. In recent times, several advanced design concepts for this class of gaseous detectors have been successfully implemented. These are specially aimed at enhancing the rate handling capabilities and position resolution of these detectors in the high energy collider experiments. Microstrip gas counters (MSGC) [2] and major variants of micropattern gas detectors (MPGD), like MICROMEGAS [3] and GEM [4] based detectors are being successfully developed to replace the multiwire proportional counter (MWPC).

In the collider experiments of high energy physics, the challenge lies in the detection of energetic mesons, pions and other hadrons. These energetic minimum ionizing particles (MIPs), causing minimum ionization in the active gas volume of the detector, require an operating gas pressure of around 1 bar inside the detector volume. The energy deposited in the active volume even by the MIPs is quite large

at this pressure to get a measurable electrical signal. Thicknesses of the absorbers in the path of the energetic particles become minor issues and hence one can afford to use the MWPC configuration having a grid of uniformly spaced thin wires kept at a positive potential (anode grid) and placed between two parallel conducting plates at ground potential (cathode plane). The more recent variants of MWPC like MSGC, MPGD, etc. which pose additional absorber thickness in the path of the charged particles can also be used for this purpose.

However, in nuclear physics experiments requiring detection of heavy ions like evaporation residues, fission fragments, etc. at low energies ($\leq$10 MeV/A), the specific energy losses of heavy ions are orders of magnitude larger than that of MIPs and hence, the absorber thickness in the path of the ions (e.g. the thin windows which separate the active gas volume of detector from the high vacuum outside and the electrode films), becomes a major issue in deciding the detector configuration. More advanced type of detectors like MSGC and MPGD cannot be adopted for the detection of low energy heavy ions as the absorber thicknesses in the path of the impinging heavy ions become very large. However, for lighter ions (viz. from proton to oxygen) at low energies, use of low pressure MWPCs have been pioneered by Breskin [5]. Very thin foils ($\sim$0.4 μm thickness), two for the cathode strips and two more as pressure foils, were used. Some of the outstanding properties of low pressure MWPC, like excellent time resolution ($\sim$100 ps) and position resolution ($\sim$300 μm), have made it the detector of choice for tracking and time of flight (TOF) measurements at low energies.

For the detection of heavier ions at low energies, even the number of thin foils quite often need to be reduced. Thickness of the window materials and the metalized foil electrodes, usually made of mylar or polypropylene, can seldom be made less than one micron thick, which makes it difficult to use the MWPC-type detector. Also the detectors must be operated at a lower gas pressure (typically a few millibar). This sets much more stringent requirement if the multiwire counter is the first element of a multi-element detector telescope. Therefore, for low pressure operation of these detectors, multiple thin wire grids with very good transmission efficiency replace the thin foil electrodes of the MWPC. This configuration, known as parallel grid avalanche counter (PGAC), and first suggested and implemented by Fabris *et al* [6], was found to give a good time resolution of 200–400 ps (FWHM) for the fission fragments, but the best time resolution ($<$200 ps) was achieved for the parallel plate avalanche counter (PPAC) of equivalent dimensions and operating condition. Inferior time resolution in PGAC was attributed to the non-uniformity of electric field inside the active detector volume caused by the grid structure. A comparative investigation on grid mesh structure demonstrated that with 45 lines per inch mesh grid having $\geq$90% transmission efficiency, one gets the best time resolution ($\sim$220 ps). It was also noted in the above reference that in the case of mixed foil and grid electrode configurations, better time resolution was obtained for foil cathode–grid anode configuration suggesting that the non-uniformity of electric field near the cathode contributes to worsening of time resolution. In order to corroborate these observations, it is important to know the electric field configuration inside the active detector volume for various detector geometries, and study the dynamical evolution of secondary electron avalanche which contributes to the signal generated.

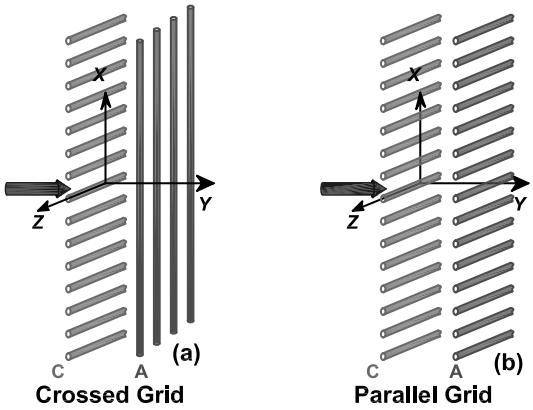

Figure 1. The crossed (**a**) and the parallel (**b**) grid configurations and the corresponding coordinate systems. Ionizing radiation enters the detectors along the y-axis as shown by arrows.

The electric field configuration in a multiwire proportional counter was first analytically calculated by Erskine [7], and incorporated into the well-known GARFIELD programme [8]. The approach followed is based on an extension of computation of complex electrostatic potential due to a single infinitely long line charge, placed between a pair of parallel grounded semi-infinite electrodes. This essentially gives rise to a two-dimensional electrostatic field configuration, which can be used to compute the dynamics of secondary electron generation caused in the wake of an ionizing radiation penetrating through the active detector volume. Several such computations give us a good insight into the performance of the MWPC detector in terms of its characteristic properties like gain, time resolution and position sensitivity. A major limitation of the analytical approach is in handling finite lateral extent of the detectors and therefore, a three-dimensional electrostatic field calculation in this case is still an open problem. Recently, a few attempts at numerical computations based on and boundary element method (BEM) or nearly exact BEM (NEBEM) [9] were made. These studies are essential in order to optimize the detector configuration suited for the targeted experiment. Similar calculations for the PGAC are also essential in order to validate its performance on more quantitative footing against that of the benchmark detectors like PPAC and MWPC. However, such studies are not yet done and will be attempted in this work.

The paper is organized as follows. Electric field distribution in the PGAC is evaluated and studied as described in §2. Monte Carlo simulation method followed in this calculation is detailed in §3, and the simulation results are discussed in §4.

2. Electric field configuration

Configuration of the PGAC detector considered for the Monte Carlo simulation is schematically shown in figure 1. It consists of a cathode grid (C) made of equispaced wires of diameter d_1 and inter-wire spacing s. The anode grid (A) is also

made of equispaced wires of diameter d_2, of the same wire spacing, and separated by a distance L from the cathode. The orientation of the wires of the two grids may either be perpendicular (crossed grid) or parallel (parallel grid) to each other. Electrostatic potential at any field point and the charge per unit length for one such grid plane biased at a fixed potential and placed equispaced (gap = L) between two ground planes can be calculated [7]. The electrostatic potentials in the two configurations can be obtained from the above by applying the priciple of superposition. The electric field components can be calculated from the electrostatic potentials. For the crossed grid configuration, it is obtained as

$$
\begin{aligned}
E_x &= \frac{\pi V_{01}\sin(\frac{2\pi x}{s})}{2s[\frac{\pi L}{s}-\ln(\frac{\pi d_1}{s})][\sin^2(\frac{\pi x}{s})+\sinh^2(\frac{\pi y}{s})]},\\
E_y &= \frac{\pi}{2s}\left[\frac{V_{01}\sinh(\frac{2\pi y}{s})}{[\frac{\pi L}{s}-\ln(\frac{\pi d_1}{s})][\sin^2(\frac{\pi x}{s})+\sinh^2(\frac{\pi y}{s})]}\right.\\
&\quad\left.+\frac{V_{02}\sinh(\frac{2\pi(y-L)}{s})}{[\frac{\pi L}{s}-\ln(\frac{\pi d_2}{s})][\sin^2(\frac{\pi z}{s})+\sinh^2(\frac{\pi(y-L)}{s})]}\right],\\
E_z &= \frac{\pi V_{02}\sin(\frac{2\pi z}{s})}{2s[\frac{\pi L}{s}-\ln(\frac{\pi d_2}{s})][\sin^2(\frac{\pi z}{s})+\sinh^2(\frac{\pi(y-L)}{s})]},
\end{aligned}
\tag{1}
$$

where V_{01} and V_{02} are the applied cathode and anode grid potentials. The crossed grid configuration generates a three-dimensional field distribution. In contrast, for the parallel grid configuration, non-zero electric field exists in two dimensions only. The x- and y-components are given by

$$
\begin{aligned}
E_x &= \frac{\pi}{2s}\left[\frac{V_{01}\sin(\frac{2\pi x}{s})}{[\frac{\pi L}{s}-\ln(\frac{\pi d_1}{s})][\sin^2(\frac{\pi x}{s})+\sinh^2(\frac{\pi y}{s})]}\right.\\
&\quad\left.+\frac{V_{02}\sin(\frac{2\pi x}{s})}{[\frac{\pi L}{s}-\ln(\frac{\pi d_2}{s})][\sin^2(\frac{\pi x}{s})+\sinh^2(\frac{\pi(y-L)}{s})]}\right],\\
E_y &= \frac{\pi}{2s}\left[\frac{V_{01}\sinh(\frac{2\pi y}{s})}{[\frac{\pi L}{s}-\ln(\frac{\pi d_1}{s})][\sin^2(\frac{\pi x}{s})+\sinh^2(\frac{\pi y}{s})]}\right.\\
&\quad\left.+\frac{V_{02}\sinh(\frac{2\pi(y-L)}{s})}{[\frac{\pi L}{s}-\ln(\frac{\pi d_2}{s})][\sin^2(\frac{\pi x}{s})+\sinh^2(\frac{\pi(y-L)}{s})]}\right].
\end{aligned}
\tag{2}
$$

Magnitude of the electrostatic field $|\vec{E}(\vec{r})|$ at different field points inside the detector volume for the two grid configurations are shown in figure 2. The detector parameters chosen for the calculation are: $d_1 = 40$ μm, $d_2 = 25$ μm, $L = 5$ mm and $V_{02} = -V_{01} = 300$ V. For the crossed grid, $x = 1.1$ mm is chosen to calculate $|\vec{E}|$. The electric field in the bulk volume of the detector is $\approx$104 V $\cdot$ mm^{-1} for both grid configurations. The corresponding electric field magnitude for the PPAC configuration is 120 V $\cdot$ mm^{-1}, which is as expected. It is to be noted that in the PPAC, the electric field in the bulk volume is uniform throughout and has to aid generation of secondary electrons throughout the detector volume. However, the

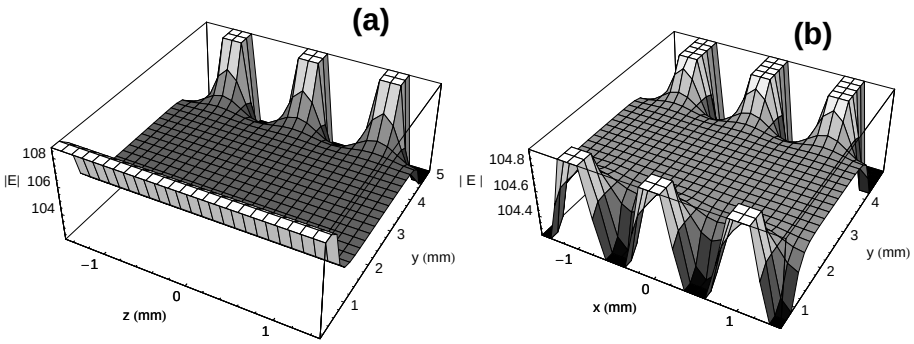

Figure 2. Electrostatic field plots in three dimensions for (**a**) crossed grid and (**b**) parallel grid, computed using parameters given in the text. $|E|$ is expressed in $\mathrm{V \cdot mm^{-1}}$.

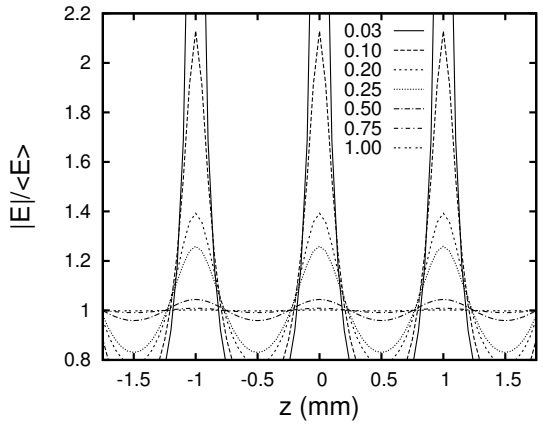

Figure 3. Field non-uniformity is plotted as a function of z. The different lines shown correspond to different distances (along y in mm) of the field points from the anode plane, as indicated by the labels in the figure.

increase in electric field magnitude in the vicinity of the anode wires in the PGAC can be well above that can be sustained in the equivalent PPAC detector before breakdown occurs. This is observed from the field non-uniformity plots shown in figure 3 for the crossed grid configuration. The ratio $|\vec{E}|/\langle E\rangle$, where $\langle E\rangle$ is the magnitude of the uniform electric field in the bulk volume of the detector, indicates deviation from the uniform field as it would be expected in a PPAC. It is found that, for the given grid configuration and the applied potentials, the equivalent PPAC electric field magnitude is reached at a distance of $\sim$0.25 mm from the anode grid for the PGAC (indicated by the dotted line in the figure). This distance from the anode corresponds to $\sim$10 times the anode wire diameter. This is expected to cause localization of avalanche near the anode wires of the PGAC.

3. Avalanche formation and propagation

A Monte Carlo program is developed and utilized for the simulation of avalanche formation and its propagation inside the PGAC detector. In this program, a parallel beam of energetic charged particles with uniform random distribution in the transverse direction (y-axis in figure 1) is allowed to fall on the detector. Alternatively, a diverging beam of particles having a Gaussian profile can also be allowed to enter the detector. Isobutane gas at a typical pressure of 5–20 mbar is taken as the active medium of the detector. The gas thickness inside the detector is divided into layers of equal thickness for calculating the energy deposited at each step along the track. Since our aim is to optimize the detector for the detection of low energy heavy ions, the evaporation residues in particular, we have primarily considered a beam of ^{212}Ra having 10–20 MeV energy falling on our detector. Low energy heavy ions such as ^{12}C (10–70 MeV), ^{102}Mo (20–80 MeV as fission fragments), ^{19}F (80–140 MeV) and ^{4}He (2–10 MeV α-particles) have also been included in the calculations specifically to check for consistency and dependence on the ion species and consequent primary ionization. The amount of energy deposited at every step inside the gaseous medium of the detector is calculated using the specific energy loss computed by the code SRIM [10]. Assuming that most of the energy deposited goes into ionization, we calculate the number of electron–ion pairs produced. Propagation of these electrons in the electric field inside the detector is considered primarily as a combination of drift motion and thermal diffusion through the medium. In the simulation calculation, it is assumed that (a) there is no electronegative impurity gas (oxygen, fluorine, nitrogen, etc.) inside, (b) space charge build-up inside the detector is negligible and (c) no recombination of electrons and positive ions takes place inside the detector volume. The latter condition is usually fulfilled by the presence of a large electric field inside the detector volume.

The gas amplification factor (M) commonly termed as gas gain, defined as the ratio of the number of secondary electrons produced by each primary electron, is dependent on the geometry, the applied potential, the gas and its pressure. At any point r_0 along the track, the gas gain M is given by

$$M = \exp\left[\int_{r_\mathrm{i}}^{r_0} \alpha(r)\mathrm{d}r\right], \tag{3}$$

where r_i is the initial position of the primary electrons and $\alpha(r)$ is the first Townsend coefficient. The gas gain calculation depends on this single-most important parameter. The quantity $\alpha(r)$ is approximately given by the Korff parametrization:

$$\frac{\alpha(r)}{p} = A\exp\left[-\frac{B}{E(r)/p}\right], \tag{4}$$

where A and B are the constants, and $E(r)$ and p are the magnitude of electric field and the pressure inside the detector. The quantity $\alpha(r)$ is calculated under different conditions and approximations on the electric field configuration, and is found to yield different expressions in different regions of reduced electric field, E/p [11] and also in uniform and non-uniform electric field. A compilation of such calculations is given in ref. [12]. However, it was established by Zastawny

[13] that one can use the pametrization of eq. (4) for the calculation of $\alpha(r)$ in a non-uniform field using a modified set of A and B coefficients, which are obtained from fit to the experimental data. In our simulation calculations, we have taken $A = 2.05\ \mathrm{mm}^{-1} \cdot \mathrm{mbar}^{-1}$, $B = 30.63\ \mathrm{V} \cdot \mathrm{mm}^{-1} \cdot \mathrm{mbar}^{-1}$, which were obtained from measurements done at operating pressures nearer to our chosen values.

For a single event, all the primary and the secondary electrons contributing to the avalanche build-up, are taken into account. Since the transit time of the heavy ions passing through the detector is negligibly small, the primary ionization at each layer is assumed to take place simultaneously. The onset of production of secondary electrons is obtained from eqs (3) and (4). Motion of the primary and the secondary electrons from each layer is followed through the electric field in equal time steps. The average time required by a primary electron to reach the anode from its point of production is calculated. This time interval is divided into equal time steps ($\sim$ a few picosec) for the above purpose. The Cartesian velocity components at any point are calculated by taking the drift motion in the electric field and thermal diffusion along the corresponding axes into account. For isobutane gas at low pressure, these are calculated from the data given in ref. [14]. The electron avalanche tracks are found to be converging towards the individual anode wires due to localization of electric field. Termination of the avalanche tracks near the anode wires is done in two ways. The electron tracks, which are within ± 0.3 mm of the anode wire, are found to bend and reach the anode wire surface where the tracks are terminated. For the rest of the tracks, the drift motion is found to extend beyond the anode plane, and turn around towards the nearest anode wire surface, resulting in circular motion around the wire, followed by termination. Observation of such motion from the simulation studies in a low pressure single wire proportional counter was also done by Pruchova and Franek [15]. The gain for the event, defined as the ratio of the accumulated total number of electrons produced up to termination of the avalanche track, to the total number of primary electrons produced by ionization, was calculated. It may be pointed out that the gas gain is usually taken as the ratio of the number of secondary electrons produced in the avalanche to the number of primary electrons created at the entry point to the detector volume (cathode plane in our detector geometry) [16]. However, we have considered an average gain calculated by taking into account all the primary electrons produced along the ion track. This is expected to be less than the gas gain. We have found that the average gain is about one order of magnitude smaller than the gas gain defined as above. The average gain also does not depend on the primary ionization which we have evaluated for a range of ion species mentioned before. The variation is found to be less than 0.2% for different ion species and energies for a fixed detector bias voltage.

In order to better understand the impact of field localization effect, we define a parameter called volume fraction V_{F}, defined as the ratio of the detector volume where secondary electron generation occurs, to the total volume of the detector. It is, thus, a quantitative measure of the active volume of the detector contributing to the avalanche formation. Response of the PGAC detector will depend on this active volume, which may be termed as the volume response, and also on the electric field configuration, which may be termed as the field response. In calculating the V_{F}, we choose small cross-sectional area comparable to that offered by the wires so that the effect of field localization near the wires can be studied. However, the choice

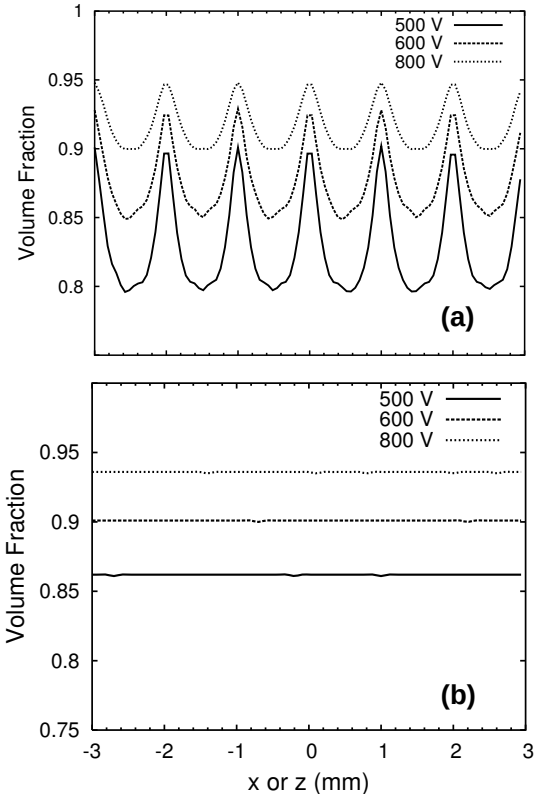

Figure 4. Dependence of the volume fraction on the x- and z-coordinates of the incident heavy ions are shown in (**a**) and (**b**) respectively. The different plots correspond to different applied bias potentials indicated in the figures.

of this cross-sectional area does not have any influence on V_F. For the crossed grid configuration, the variation of V_F along x (i.e. perpendicular to the cathode wires) is plotted in figure 4a for different applied potentials across the grids. From the figure, it is evident that V_F carries the fingerprint of the cathode wire grid structure. The average value of V_F, however, increases but the RMS deviation decreases as the applied bias potential is increased. This indicates that in the PGAC, the volume response will depend more on the cathode grid structure at relatively lower applied bias potentials, but it tends to be more uniform at higher applied bias potentials. A similar plot of V_F as a function of position (z) along the anode plane perpendicular to the anode wires is shown in figure 4b. No major dependence of V_F on the anode structure can be seen indicating that the anode structure has virtually no influence on the volume response of PGAC with crossed grid configuration. For the parallel grid configuration, there is no difference in the volume response on the two different grid structures, as expected. However, the actual response will depend more on the field response of the detector as we will find in the next section.

We have also probed the influence of the cathode wire diameter on the volume response. Keeping the same bias potential across the detector, we observe that V_F

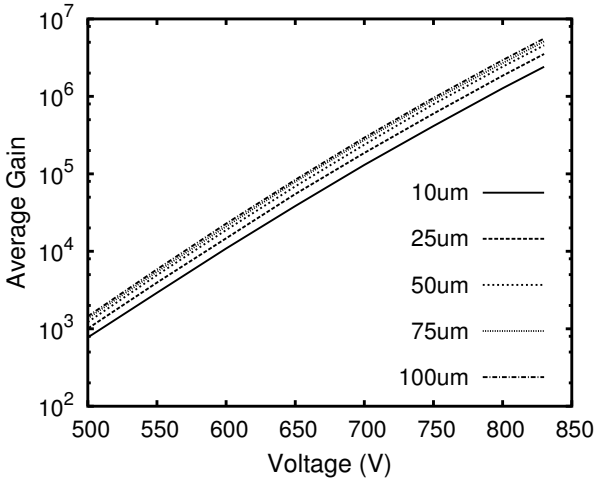

Figure 5. Dependence of the average gain on the applied bias voltage for the crossed grid configuration. The gain curves for different anode wire diameters (labelled in the figure) are shown.

decreases with the decrease of the cathode wire diameter. The volume response, thus, appears to be more uniform for larger cathode wire diameters, though the effect is only marginal (by ∼1%) for a change of diameter from 10 μm to 75 μm.

4. Results

In the Monte Carlo simulation calculation, the average gain is computed by averaging the gain for all the individual hits taking place over a 10 mm × 10 mm area of the detector. The average gain increases exponentially with the applied bias voltage as shown in figure 5. It is computed for different anode wire diameters as shown in the same figure. The average gain is higher for larger anode wire diameter, indicating that the larger the surface area of the anode grid wires, the more is the uniformity and the magnitude of the drift electric field in the bulk volume of the detector, which contributes to the enhancement of gain. The sharper rise in electric field near the anode wires of decreasing diameter does not influence the average gain at this low pressure operation. Davydov *et al* [17] had observed similar dependence at comparable gas pressure (10 mbar) from experiments done with single wire proportional counter. We have also observed the same dependence of the calculated average gain on anode wire diameter for both the crossed and the parallel grid configurations.

The choice of grid configuration for the PGAC detector is guided by two major criteria: (a) overall gain of the detector and (b) uniformity of spatial response. The latter criterion is of importance for judging the suitability of the detector as a position sensitive device. We have calculated the average gain of the PGAC detector for the crossed and the parallel grid configurations. All other geometrical parameters, gaseous medium and its pressure are kept the same. Variation of the

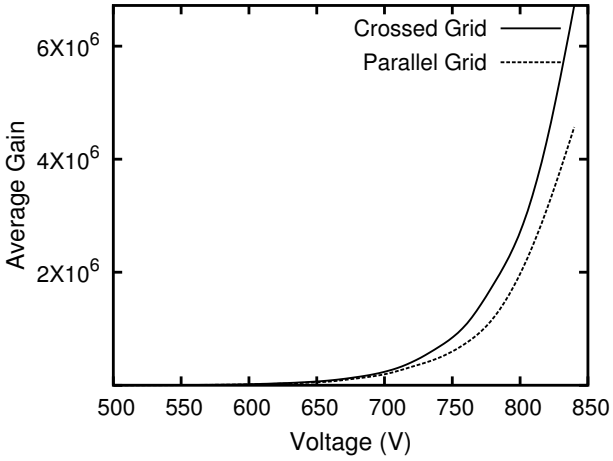

Figure 6. Average gain for the two grid configurations are plotted as a function of applied voltage. The detector medium, pressure and geometrical parameters are the same as mentioned earlier.

average gain with applied bias voltage for the two configurations are plotted in figure 6. It is seen that the average gain is marginally higher for the crossed grid configuration at bias voltages above 700 V. This corresponds to a reduced electric field $E/p \approx 23\ \mathrm{V \cdot mm^{-1} \cdot mbar^{-1}}$ in the bulk volume of the PGAC. At lower bias voltage, the gains are almost the same. From the available data on these kind of detectors, we find that the bulk of the PGAC detector would operate in the region of limited proportionality above 700 V bias voltage, while the strong electric field localized near the wires would drive the neighbouring region to avalanche, causing gain variation sensitive to the magnitude of the localized electric field, which is different for the two grid configurations, especially near the cathode grid. In other words, we find that the field response wins over the volume response in causing a marginal increase of the average gain for the crossed grid at higher applied bias voltages.

In order to look at the above aspect in more detail, we have calculated the gain for the individual charged particle tracks for both the grid configurations. The tracks are randomly chosen to be incident perpendicular to the detector over a 10 mm $\times$ 10 mm area. These gains, calculated at an applied bias potential of 800 V for the crossed grid configuration, are plotted as a function of z in figure 7. The same is plotted as a function of x for the parallel grid configuration in the same figure. The detector parameters chosen for the calculations are: $d_1 = 40\ \mu$m, $d_2 = 25\ \mu$m, $L = 5$ mm, and isobutane gas pressure inside is 5 mbar. For both the configurations, the gain is found to vary in magnitude between $\sim 9 \times 10^5$ and $\sim 6 \times 10^6$, with the maximum nearest to the anode wires and minimum mid-way between the wires. The spatial distribution of gain is somewhat different for the two configurations. In the case of parallel grid, the peaks near the anode wires appear to be narrower than in the case of crossed grid. The average gain over the 10 mm span of the PGAC detector, obtained for the simulated data shown in figure 7 is found to be: $(2.71 \pm 1.36) \times 10^6$ for the crossed grid and $(1.97 \pm 1.18) \times 10^6$ for the parallel grid.

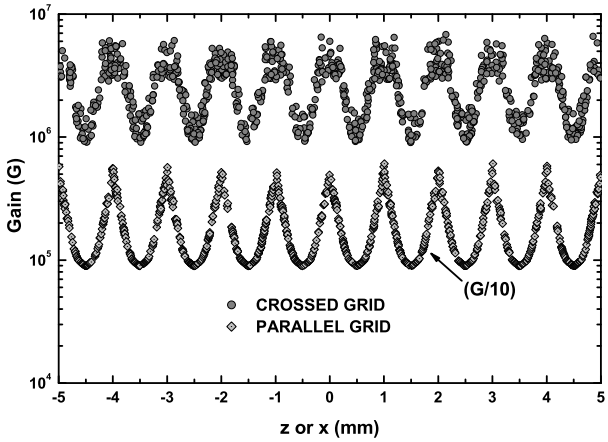

Figure 7. Plots of gain as a function of position of the tracks of incident particles for the crossed grid and the parallel grid configurations.

This marginally higher gain for the crossed grid configuration (also evident from figure 6) can be attributed to the field response of the PGAC detector. To look at it in more detail, we have calculated the average FWHM of the gain peaks for both the configurations calculated over the 10 mm $\times$ 10 mm area. The average FWHM for the two configurations are: 0.44(0.03) mm and 0.29(0.03) mm for the crossed grid and parallel grid configurations respectively. Therefore, the gain for the individual charged particle tracks are relatively higher for the crossed grid, which results in higher average gain. Thus, the crossed grid configuration is expected to have a more uniform spatial response than the parallel grid. To use the PGAC as a position sensitive detector, a position sensing grid is usually placed between the anode and the cathode grids. The induced charge signal produced on the position grid wires are read out either from individual sense wires, or using resistive chain or delay line read-out technique. Based on our results, we can conclude that the crossed grid configuration, with better uniformity of response would be preferred over parallel grid for developing such a position sensitive detector.

5. Summary

We have studied the crucial role played by the electric field distribution in the formation of electron avalanche and the dynamics of its propagation inside parallel grid avalanche counters. The electrostatic fields for the crossed and the parallel grid configurations are calculated from the derived analytic expressions. The finite boundary or edge effects are not considered in this calculation. Based on the above field calculations, and using Monte Carlo simulation technique, we have systematically evaluated the volume response and field response of the PGAC at low pressure of isobutane gas as active detector medium. A weaker electric field in the bulk volume of the PGAC (i.e. away from proximity of the wires of the two grids) is found to play a major role in deciding the response of the detector at lower bias

potentials. The higher electric field near the wires causes an exponential increase in gain at higher bias potentials. Dependence of volume response and gain on the wire diameters are also evaluated. We find that wires with larger diameter result in higher gain. We have also observed that the average gain is higher for the crossed grid than that for the parallel grid at higher bias potentials. This is a consequence of the difference in the electric field near the wires for the two configurations. We have also observed that the gain is relatively more uniform for the crossed grid, making it a better choice for the use of PGAC as a position sensitive device for the detection of heavy ions.

References

[1] G Charpak, R Bouclier, T Rressani, J Favier and C Zupancic, *Nucl. Instrum. Methods* **62**, 262 (1968)
[2] A Oed, *Nucl. Instrum. Methods* **A263**, 351 (1988)
[3] Y Giomataris, Ph Rebourgeard, J P Robert and G Charpak, *Nucl. Instrum. Methods* **A376**, 29 (1996)
[4] F Sauli, *Nucl. Instrum. Methods* **A386**, 531 (1997)
[5] A Breskin, *Nucl. Instrum. Methods* **196**, 11 (1982)
[6] D Fabris, G Fortuna, F Gramegna, G Prete and G Viesti, *Nucl. Instrum. Methods* **216**, 167 (1983)
[7] G A Erskine, *Nucl. Instrum. Methods* **105**, 565 (1972)
[8] http://garfield.web.cern.ch/garfield/
[9] N Majumdar and S Mukhopadhyay, *Nucl. Instrum. Methods* **A566**, 489 (2006)
[10] J F Ziegler and J P Biersack, Copyright: SRIM.com, 2003, All Rights Reserved
[11] V Palladino and B Sadoulet, *Nucl. Instrum. Methods* **128**, 323 (1975)
[12] I Krajcar Bronić and B Grosswendt, *Nucl. Instrum. Methods* **B142**, 219 (1998)
[13] A Zastawny, *Nucl. Instrum. Methods* **A385**, 239 (1997)
[14] A Peisert and F Sauli, CERN Report, 84-08, 13 July 1984, Geneva
[15] H Pruchova and B Franek, *Nucl. Instrum. Methods* **A366**, 385 (1995)
[16] A Breskin, A Buzulutskov, R Chechik, D Vartsky, G Malamud and P Miné, *Nucl. Instrum. Methods* **A344**, 537 (1994)
[17] Yu I Davydov, R Openshaw, V Selivanov and G Sheffer, *Nucl. Instrum. Methods* **A545**, 194 (2005)